On the interplay between MHD instabilities and turbulent transport in magnetically confined plasmas

On the interplay between MHD instabilities and turbulent transport in magnetically confined plasmas

K. Ida[1, 2]

[1] *National Institute for Fusion Science, National Institutes of Natural Sciences, Toki, Gifu 509-5292, Japan*
[2] *The Graduate University for Advanced Studies, SOKENDAI, Toki, Gifu 509-5292, Japan*

(Dated: September 18, 2019)

Interplay between MHD and turbulence is an interesting topic in magnetically confined plasma and solar plasma. Recently experimental observations below suggest the coupling and interplay between MHD and turbulence in magnetically confined toroidal plasmas. 1) Turbulence spreading into the magnetic island, 2) self-organized change in topology and turbulence in magnetic island, 3) flow damping by stochastic magnetic field, 4) trigger mechanism for the MHD bursts, 5) impact of MHD bursts on the ion velocity distribution and potential, and 6) turbulence exhausts at the MHD burst event. In this paper, experimental evidence for the interplay between MHD and turbulence in toroidal plasmas is reviewed. The physics mechanism of the interplay and a possible link to astrophysical plasma physics are also discussed.

PACS numbers:

I. INTRODUCTION

The interplay between MHD and turbulence is an interesting topic in magnetically confined plasma and solar plasma research. Fast reconnection of magnetic field in solar flares is well known. However the mechanism is not fully understood. Turbulence in the current sheet is a strong candidate to explain fast reconnection in solar flares [1, 2]. In magnetically confined plasmas, MHD instabilities and electrostatic turbulence have been investigated independently. No coupling between the electrostatic turbulence and MHD instability is assumed.

However, recent experimental observations below suggest the coupling and interplay between MHD and turbulence in magnetically confined toroidal plasmas [3], turbulence spreading into the magnetic island [4], self-organized change in topology and turbulence in magnetic island [5], flow damping by stochastic magnetic field [6], trigger mechanism for the MHD bursts [7], impact of MHD bursts on the ion velocity distribution and potential [8, 9], and turbulence exhausts at the MHD burst event [10]. Evidence for the interplay between MHD and turbulence in toroidal plasma is reviewed and the physics mechanism of the interplay is also discussed in section II. For example, in the heat pulse experiment in DIII-D tokamak plasma, the turbulence increase occurs after the arrival of the heat pulse with a significant delay at the X-point, while it occurs before the heat pulse radial propagation at the O-point of the magnetic island. This is due to the turbulence spreading from the X-point to the O-point of the magnetic island faster than the heat pulse determined by the transport time scale inside the magnetic island. In D-IIID tokamak, two states of magnetic islands are observed. The 'high-accessibility' state is when the heat pulse propagating from outside a magnetic island can penetrate inside the magnetic island, while the 'low-accessibility' state is when penetration of the heat pulse into the magnetic island is prevented at the boundary. These oscillations between these states are self-regulated and the change in magnetic topology such as stochastization of the magnetic field at the boundary of the magnetic island is one of the possible mechanisms for this self-regulated oscillation. A self-regulated oscillation of the topology and transport inside the magnetic island is observed owing to the interplay between the MHD and turbulence. In Large Helical Device (LHD) helical plasma, anomalous flow damping is observed related to the stochastic magnetic field in the plasma core, which suggests the interplay between MHD and turbulence in plasma.

More recently, a strong MHD burst is found to have been triggered by the non-modal (no toroidal and no poloidal periodic number) localized plasma deformation. Here, non-modal means that there is no clear helical structure characterized by the low order toroidal and poloidal periodic number usually expressed by n/m at the rational surface. The non-modal perturbation has solitary structure and is highly localized in toroidal and poloidal direction. The perturbation with solitary structure is observed near the plasma edge when the edge localized mode (ELM) activities are excited, and is also known as a finger structure [11, 12]. This MHD burst causes the distortion of ion velocity distribution and large potential due to energetic ion loss. This MHD burst also causes the rapid radial propagation of turbulence from plasma core to SOL region. This is also clear evidence for the interplay between MHD and turbulence. A new experimental result on the impact of an MHD burst on plasma flow and turbulent transport as evidence for interaction between MHD and turbulence is discussed in section III.

Figure 1 shows a diagram of physics elements of interactions between topology and MHD and interactions between turbulence and plasma flow. The interaction between flow shear of parallel, $E \times B$ flow, and zonal flow

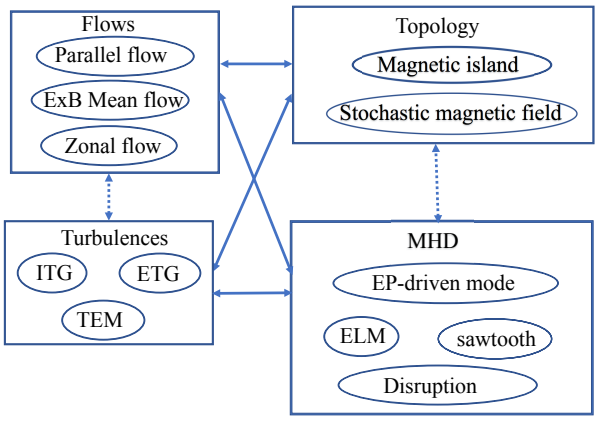

FIG. 1: Diagram of physics elements of interactions between plasma flow, turbulence, topology, and MHD.

has been discussed since the strong $E \times B$ flow shear was found in the pedestal region in the H-mode plasma. The flow shear contributes to the suppression of turbulence shearing effect, and flow shear has been recognized to be a key element in the feedback loop of formation of edge and internal transport barrier. Recently, work on the interaction between topology and MHD where the conclusion is that the plasma self-organizes by triggering an internal bifurcation of magnetic island chains [13, 14]. However, there are few experiments reported on the interactions between turbulence and topology or MHD and the interaction between topology and MHD in the toroidal plasma.

MHD instability causes the change of magnetic topology in the plasma. The magnetic island and the stochastic magnetic field are topology effects commonly observed in a toroidal plasma. The oscillations are observed in the magnetic probe signal or temperature due to the plasma rotation. The oscillation frequency is finite in the laboratory frame but zero in the plasma frame. Therefore, when the plasma does not have rotations, oscillations owing to this topology effect disappear. In contrast, the MHD has a characteristic frequency of the oscillation of the magnetic field in the plasma frame and sometimes grows non-linearly and triggers the collapse of plasma. Energetic particle driven modes, Edge localized mode (ELM), the sawtooth crash, and disruptions are included in this category.

II. INTERPLAY BETWEEN TURBULENCE AND TOPOLOGY

A. Turbulence spreading into magnetic island

In the local transport model, the turbulence level in the plasma is assumed to be determined by the local plasma parameters such as temperature and density, their gradients, and the magnetic field and potential structure (magnetic shear and radial electric field shear). However, various non-local phenomena that cannot be explained by local transport model have been observed in experiments in toroidal plasma [15]. These experimental results are evidence that the local closure of flux-gradient (turbulence-gradient) relation is violated. Several of the mechanisms causing the violation of these relations have been proposed in theory. Coupling between the turbulence of meso- or long-range correlation and micro turbulence have been proposed to explain the strong core-edge coupling of turbulence and transport observed in experiment. In avalanche model, a strong nonlinearity of the growth rate of the micro-scale turbulence can cause a simultaneous fast radial propagation of both micro turbulence and gradients, and consequences in ballistic transport and supper diffusion. The turbulence coupling and turbulence spreading are the most likely mechanisms causing the non-local transport. Recently, turbulence spreading from the pedestal region to the scrape off layer (SOL) is expected to be beneficial in broadening the SOL power decay length [16–21]. Therefore, the experimental identification of turbulence spreading becomes one of the crucial issues in edge transport.

In spite of the importance of the turbulence spreading, there are only a few measurements on turbulence. This is because the separation of the turbulence origin (spreading turbulence and locally driven turbulence) is impossible in the usual turbulence measurements. The novel analysis of turbulence to distinguish the origin of the turbulence with the modulation of bias was reported from TJ-II. The time evolution of free turbulent energy $\langle\tilde{n}^2\rangle$ (where $\tilde{n}$ = n - $\langle n\rangle$) is obtained from the radial part of the continuity equation by neglecting cross-field coupling and damping as well as the effect of background flows as [22]

$$\frac{1}{2}\frac{\partial}{\partial t}\langle\tilde{n}^2\rangle \;=\; -\langle\frac{\partial n}{\partial r}\rangle\langle\tilde{v}_r\tilde{n}\rangle - \frac{1}{2}\frac{\partial}{\partial r}\langle\tilde{v}_r\tilde{n}^2\rangle \qquad (1)$$

The angular brackets $\langle ...\rangle$ indicate a running average over a time interval much larger than the turbulence correlation time. First term is a product of the turbulent particle flux and density gradient and the second term is a diffusion of turbulent energy. With the normalization by the local turbulence amplitude, $\langle\tilde{n}^2\rangle$, two rates of turbulence are defined. One is the rate of turbulence drive due to the density gradient as

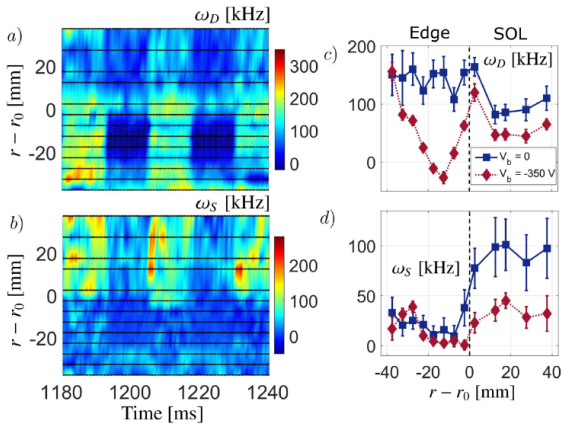

FIG. 2: Rates of (a)(c) local turbulence drive and (b)(d) the turbulence spreading during the edge biasing. (from figure 8 in [22]).

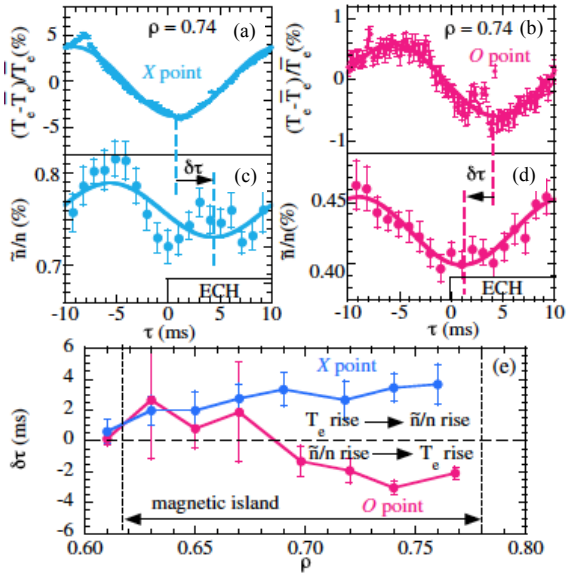

FIG. 3: Time evolution of perturbation of electron temperature at (a) X-point and (b) O-point of magnetic island, density fluctuation intensity at (c) X-point and (d) O-point of magnetic island, and (e) radial profiles of time delay of density fluctuation perturbation with respect to the electron temperature perturbation in DIII-D (from figure 3 in [4]).

$$\omega_D = -\frac{2\langle\frac{\partial n}{\partial r}\rangle\langle\tilde{v}_r\tilde{n}\rangle}{\langle\tilde{n}^2\rangle} \tag{2}$$

and the other is the rate of turbulence spreading due to the turbulence intensity gradient as

$$\omega_S = -\frac{\frac{\partial}{\partial r}\langle\tilde{v}_r\tilde{n}^2\rangle}{\langle\tilde{n}^2\rangle} \tag{3}$$

These two quantities have a quite different response to the edge biasing as seen in Figure 2. The negative edge bias of the voltage of -380 V and the modulation frequency of 40 Hz during the discharge (bias is off-on-off-on-off about 1180 - 1240 ms). The rate of the turbulence locally driven, ω_D inside LCFS ($r < r_0$), is significantly reduced during the on phase of edge biasing, while the reduction of the rate outside LCFS ($r > r_0$) is moderate. In contrast, the rate of the turbulence spreading, ω_S is significant outside LCFS ($r > r_0$), although there is almost no impact inside LCFS ($r < r_0$). The experimental data clearly shows the turbulence locally driven is suppressed at the plasma edge by $E \times B$ shear produced by edge biasing, while the turbulence spreading observed in the SOL region is suppressed by $E \times B$ shear at the plasma boundary. This experiment suggested that the $E \times B$ flow shear suppress the turbulence spreading from core to SOL.

The other approach to identify the spreading turbulence is the measurement of turbulence response in the region where the local driven turbulence is expected to be small. The magnetic island is an ideal region for the spreading turbulence because there should be no driven turbulence inside the large magnetic island in which the temperature and the density flattening region are larger than the correlation length of micro turbulence. Magnetic islands define a unique region in the plasma because the temperature and density gradients which drive the turbulence are much weaker inside than that outside the magnetic island [23]. Since the heat propagation inside the magnetic island is relatively slow [24, 25], turbulence could propagate faster than the heat pulse if there is a turbulence spreading [26, 27] from X-point (or boundary) to the O-point of the magnetic island. In order to identify the spreading turbulence, the phase relation between micro turbulence intensity measured with beam emission spectroscopy (BES [28, 29]) and electron temperature measured with electron cyclotron emission (ECE) was investigated in the X-point and the O-point of the magnetic island in the heat pulse experiment produced by modulated electron cyclotron heating (MECH) in DIII-D [4]. Figure 3(a)-(d) shows time evolution of perturbation of electron temperature and density fluctuation intensity at X-point and O-point of magnetic is-

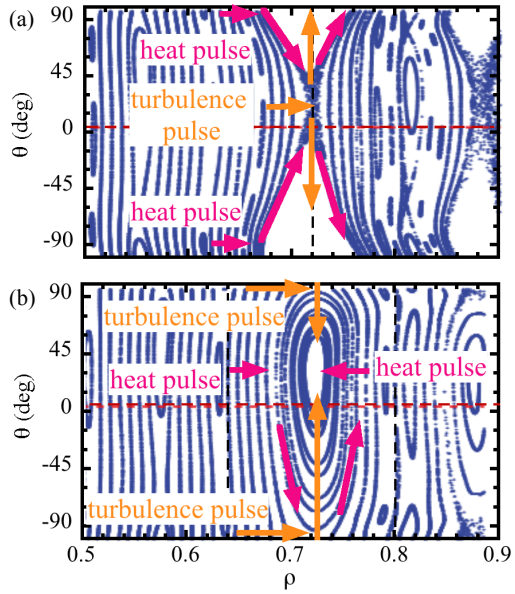

FIG. 4: Poincaré map of the magnetic field at (a) X-point and (b) O-point of the magnetic island. (from figure 4(d), 4(h) in [5] modified).

land. In this experiment, the heat pulse propagates into magnetic islands. The modulation frequency is 50 Hz and the density turbulence intensity measured with BES is integrated in the frequency range of 10 - 50 kHz. At the X-point of the magnetic island, the delay time of density fluctuation modulation with respect to the electron temperature modulation is positive. The heat pulse perturbation reaches to the X-point before the density fluctuation perturbation. In contrast, the delay time of density fluctuation modulation with respect to the electron temperature modulation is negative at the O-point of the magnetic island, which indicates that the density fluctuation perturbation reaches to the O-point before the heat pulse perturbation. As seen in figure 3(e), the negative delay time is observed in the low field side of the O-point of the magnetic island ($R > R_{\mathrm{O-point}}$, where the heat pulse propagates inward from the boundary of magnetic island to the O-point of magnetic island.

Poincaré maps of magnetic field at X-point and O-point of the magnetic island with the direction of heat pulse propagation and density fluctuation propagation indicated with arrows are plotted in figure 4. Here, the perturbation fields are calculated using the Fourier analysis module in the trip3d code [30]. In general, the electron temperature becomes constant on a magnetic flux surface because the propagation speed of heat pulse parallel to the magnetic field is an order of the electron thermal velocity and much higher than the propagation speed perpendicular to the magnetic field. In contrast, the density fluctuation is not constant on a magnetic flux surface and has poloidal asymmetry. In the normal nested magnetic flux surface, the radial propagation speed of the heat pulse is equal to that of density fluctuation. However, near the X-point of the magnetic island, the effective radial propagation speed of heat pulse (the projection of parallel heat pulse propagation to the radial direction) becomes much higher than the speed of density fluctuation propagating across the magnetic flux surface. Therefore, the heat pulse propagates to the X-point of the magnetic island before turbulence. In the O-point, the heat pulse propagates from the boundary of the magnetic island of the O-point slowly due to the low level of fluctuation inside the magnetic island (due to the lack of locally driven turbulence). However, turbulence propagating from the X-point to the O-point is faster than the heat pulse and causes the negative delay time of turbulence perturbation (turbulence increases before the heat pulse). This is clear evidence of turbulence propagation from the X-point to the O-point of the magnetic island.

B. Bifurcation of turbulence spreading at the boundary of the magnetic island

The amount of heat flux propagating through X-point or O-point depends on the velocity of heat pulse propagation at X-point or O-point region. As the heat pulse propagation becomes slow inside the magnetic island (O-point), the modulation amplitude decreases. Because the heat pulse propagates at the boundary of O-point, the delay time of the heat pulse is peaked at the O-point of the magnetic island[5]. There is a clear relation between the propagation speed (delay time) and reduction of modulation amplitude[31]. A large reduction of modulation amplitude is a result of gradual heat pulse propagation due to low turbulence level. Therefore, by measuring the modulation amplitude at O-point of the magnetic island, one can estimate the level of transport and turbulence inside the magnetic island.

The time evolutions of electron temperature measured with ECE at the O-point phase and the X-point phase of magnetic island in DIII-D are plotted in figure 5. In this experiment, the toroidal phase of the resonant magnetic field perturbation (RMP) is flipped by 180 degrees during the discharge. Here O-point (X-point) phase stands for the phase when the O-point (X-point) of the magnetic island locates at the toroidal location of ECE measurements. The heat pulse is produced by the modulation ECH and the modulation amplitude of the heat pulse is evaluated by ECE measurements. As seen in figure 5, the modulation amplitude at the X-point phase is larger than the modulation amplitude at the O-point phase. In the O-point phase, the flattening of electron temperature is observed near 0.4 keV. There is periodic change in modulation amplitude in the O-point phase which shows that the reduction of modulation amplitude is oscillating. One is the phase with moderate reduction of modulation amplitude and the other is the phase with a significant

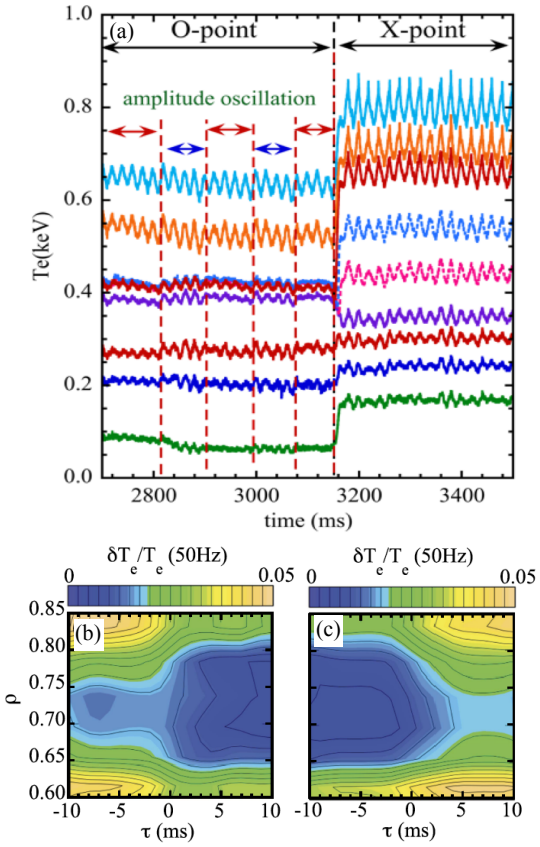

FIG. 5: (a) Time evolution of electron temperature measured with ECE at the O-point phase and the X-point phase of magnetic island and contour of modulation amplitude of electron temperature in time and space at the transition (b) from high to low accessibility states and from (c) low to high accessibility states in DIII-D. (from figure 6 in [5])

reduction of modulation amplitude. The former is called high-accessibility state of the heat pulse and the latter is called low-accessibility state of the heat pulse.

Figure 5 (b) (c) shows the contour of modulation amplitude of electron temperature in time and space at the transition (b) from high to low accessibility states and from (c) low to high accessibility states. In the high accessibility states, the modulation amplitude gradually decreases from the boundary of the magnetic island (ρ =0.64 and ρ =0.8) to O-point (ρ =0.72) of the magnetic island. In contrast, the modulation amplitude sharply drops to the low level (1 % of temperature). The time scale of the transition from high accessibility states to low accessibility states is 4 ms and the back transition from high to low accessibility states is 7 ms.

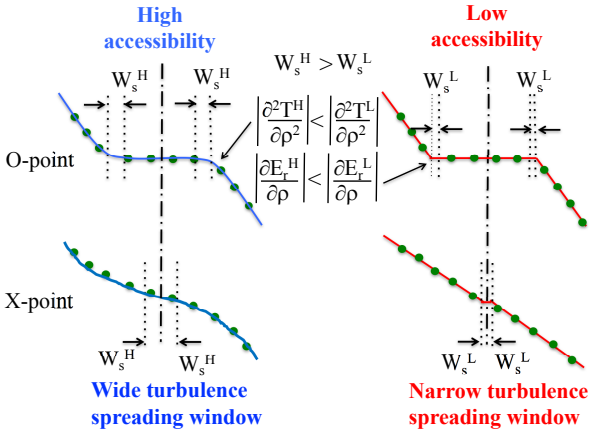

FIG. 6: Possible image of electron temperature profile at X-opint and O-point of magnetic islnad to explain the bifurcation of high and low accessibility state of magnetic island.

In general, a magnetic island is surrounded by a layer of stochastic magnetic field. Stochastization of the magnetic-field, i.e., magnetic braiding or appearance of the secondary magnetic island [34–37] can occur when the island size reaches a critical value. The width of the magnetic island in DIII-D is 15% of minor radius and large enough to expect the appearance of stochastic layer surrounding the magnetic island. When the stochastic layer surrounding the magnetic island appears, the second derivative of temperature decreases due to the enhancement of the effective radial transport. Since the $E \times B$ flow shear is roughly proportional to the second derivative of temperature, $E \times B$ flow shear decreases by the appearance of stochastic layer. Because the $E \times B$ flow shear plays an important role to prevent the turbulence spreading, the stochastisation of the field outside the island should increase the rate of spreading of turbulence into the island. Therefore, change of stochastic layer surrounding the magnetic island can be one of the candidates for the bifurcation of turbulence spreading state inside the magnetic island. Figure 6 shows the possible image of electron temperature profile at X-point and O-point of magnetic island to explain the bifurcation of high and low accessibility state of magnetic island by a simultaneous change in $E \times B$ flow shear and turbulence spreading at the boundary of the magnetic island. Turbulence measurements in bias experiment in TJ-II suggest that the turbulence spreading is reduced by $E \times B$ flow shear[22]. In theory, external $E \times B$ shearing is expected to hinder turbulence spreading [32] and the turbulence spreading is also proposed to be one of the candidates for non-local transport mechanism [15, 33]. These theoretical and experimental results support the

working hypothesis that the transition from a high to a low accessibility state is due to the change in suppression of turbulence spreading by the $E \times B$ flow shear at the boundary of magnetic island where the second derivative of electron temperature becomes significantly large.

The width of the stochastic region at the boundary of the magnetic island except for the X-point region is smaller than the correlation length of turbulence. However, at the X-point, the width of the stochastic region can be larger than the correlation length of turbulence and also should have an impact on the turbulence. The suppression of turbulence spreading results in increasing the second derivative of temperature (sharp boundary of magnetic island) and the narrow width of stochastic region (W_s) at X-point. The increase of the second derivative of temperature ($\partial^2 T/\partial r^2$) contributes to the enhancement of $E \times B$ flow and causes positive feedback. The reduction of the stochastic region width at the X-point of the magnetic island contributes to the reduction of turbulence spreading (narrow turbulence spreading window) from X-point to O-point of the magnetic island. Therefore, the low accessibility state is characterized by strong $E \times B$ shear, sharp boundary (large $\partial^2 T/\partial r^2$), and narrow stochastic region (small W_s) at X-point of magnetic island (turbulence shielding state). In contrast, the high accessibility state is characterized by weak $E \times B$ shear, broad boundary (small $\partial^2 T/\partial r^2$), and wide stochastic region (large W_s) at X-point of magnetic island (turbulence penetration state). These two states can be bifurcated because of the feedback process through the interplay between $E \times B$ shear, stochastic magnetic field and turbulence shielding.

C. Flow damping due to stochastic magnetic field

Because the interplay between the stochastic magnetic field and plasma flow is important, it is an interesting issue how the stochastic magnetic field affects the plasma flow. A heliotron plasma has a significant advantage for this study because a large stochastic region up to 60% of the plasma minor radius can be produced in the plasma core without a disruption. In general, the magnetic flux surface becomes nested when the magnetic shear is large enough, while the magnetic flux surface becomes dominated by the lowest order magnetic island (ex. 2/1 for $\iota = 0.5$)) when the magnetic shear is small. Therefore, the control of the magnetic shear is a key to producing a large region with a stochastic magnetic field near a rational surface. Tangential neutral beam has been widely used as a convenient tool of non-inductive current drive in toroidal plasma and called neutral beam current drive (NBCD). Because of the conservation of poloidal flux linking the plasma, the total current can only change on a resistive time scale. Therefore, when the NBI drives current at the plasma edge, this must induce a loop voltage that drives a compensating current in the opposite direction in the plasma core. In the high temperature plasma, this compensating current can exceed the non-inductive current by NBCD locally especially in the case of the off-axis NBCD. In LHD, this compensating current in the opposite direction becomes large enough to change the rotational transform, ι, in the direction opposite to NBCD (e.g. decrease ι for co-NBCD and increase ι for counter-NBCD) near the magnetic axis in the discharge where the direction of the off-axis NBCD is exchanged in the middle of the discharge. The exchange of NBCD in the opposite direction with each other (NBCD direction switch) has been used to change the magnetic shear at half radius of the plasma in LHD [38]. When the direction of the NBCD is switched from co-direction (parallel to equivalent plasma current direction) to counter-direction (anti-parallel to equivalent plasma current direction), the edge ι decreases due to counter NBCD but the central ι increases due to the inductive current. Then the magnetic shear at the half of the plasma minor radius decreases after the beam switch from co to counter NBCD.

Toroidal flow velocities at $r_{\rm eff}/a_{99} = 0$, 0.25, 0.5 show the abrupt drop to almost zero after the magnetic shear at the rational surface of $\iota = 0.5$ at $r_{\rm eff}/a_{99}$ decreases to ~ 0.5 as seen in figure 7 [6]. The magnetic shear at the rational surface of $\iota = 0.5$ decreases from 1.2 to 0.5 after the beam switch from co-NBI to counter-NBI at $t = 5.3$ sec. The magnetic shear is kept constant at 0.5 after $t = 5.8$ sec and abrupt drop of toroidal rotation velocity is observed at $t = 6.0$ sec. The heat pulse propagation technique is used to determine the magnetic topology. Monotonic increase in delay time of heat pulse at $t = 5.75$ sec shows that the magnetic flux surface is nested before the abrupt drop of toroidal rotation velocity (flow damping). During the phase of flow damping the delay time of heat pulse shows very large flattening region flat up to $r_{\rm eff}/a_{99} = 0.6$, which indicates that the magnetic flux surface in the core becomes stochastic[39, 40]. Later in the discharge, the toroidal rotation velocity begins to increase after $t = 6.7$ sec and partially recovers. The radial profile of delay time of heat pulse is peaked at the rational surface ($r_{\rm eff}/a_{99} = 0.5$), which indicates the disappearance of stochastic magnetic field region and the appearance of magnetic island.

Figure 7(c) shows the radial profile of onset of stochastization of the magnetic field. The stochastization of the magnetic field is initiated at the rational surface of $\iota = 0.5$ located at $r_{\rm eff}/a_{99} = 0.5$. The region of the stochastic magnetic field expands both inward and outward and the region of the stochastic magnetic becomes 20 % of the minor radius in 10 ms, which is called a partial stochastization. The outward propagation of stochastic magnetic field stops at $r_{\rm eff}/a_{99} = 0.6$ due to the higher magnetic shear towards the plasma periphery. However, the inward propagation of stochastic magnetic field continues until the stochastic magnetic field region expands to the magnetic axis in 40 ms, which is called a full stochastization.

Figure 7(d) shows the radial profile of radial electric field before the stochastization (with nested magnetic

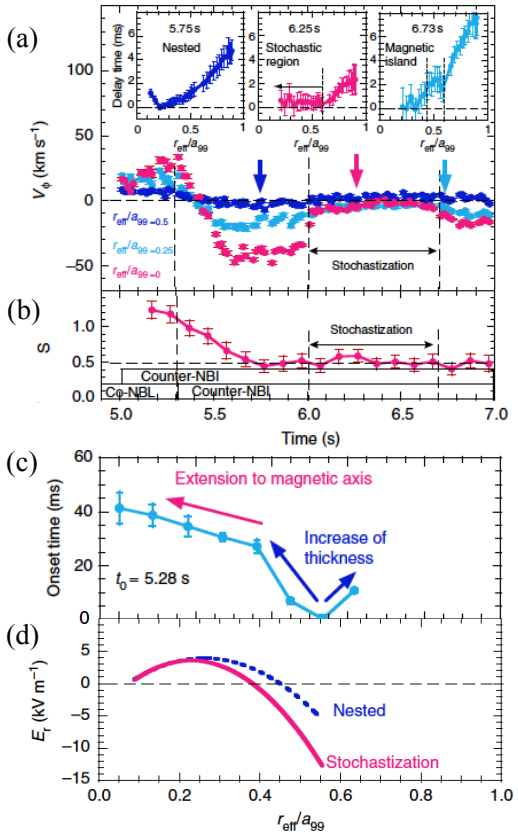

FIG. 7: Time evolution of (a) toroidal flow velocity at $r_{\rm eff}/a_{99}$ = 0, 0.25, 0.5 and (b) magnetic shear at the rational surface of $\iota = 0.5$ at $r_{\rm eff}/a_{99} \sim 0.5$ and (c) radial profile of (c) onset of stochastization of magnetic field and (d) radial electric field in LHD (from figure 1(a)(d) and figure 4(b)(d) in [6]).

flux surface) and after the stochastization of magnetic field. The positive radial electric field in the core region ($r_{\rm eff}/a_{99} < 0.4$) decreases and the negative radial electric field outside this region increases after stochastization of the magnetic field. The change in the radial electric field is more significant near the rational surface, where the dominant modes are resonant, while the flattening of the electron temperature is observed in the whole core region. This observation is consistent with the fact that the transport enhanced due to the stochastization of magnetic field is ambipolar except for the region near locations where the dominant modes are resonant [41].

The radial propagation of stochastic magnetic field is considered to be due to the consequence of interplay between stochastization and plasma flow damping. The stochastization of the magnetic field causes the strong flow damping. The plasma flow is also expected to play a role to prevent the magnetic field to become stochastic. Therefore, once the plasma flow starts to decrease due to the enhanced damping due to stochastization, the region of flow damping and stochastization expands due to the positive feedback until the stochastic region reaches to the plasma axis. In contrast, when the stochastic region starts to shrink, the plasma flow recovers due to the external torque input. The stochastic region disappears and the magnetic island appears or is completely healed (stochastization healing [42]).

III. INTERPLAY BETWEEN TURBULENCE AND MHD

The energetic particle driven MHD instabilities have been studied intensively in nuclear fusion research [43–46]. MHD instability driven by energetic particle often shows the non-linear characteristic and causes a minor collapse of the helical plasma [47, 48]. In LHD, various MHD instability driven by energetic particle is observed when the high power neutral beams ($\sim$ 30 MW) are injected into the low density ($\sim 1 \times 10^{19}$m^{-3}) target plasma [49, 50]. The minor collapse of the plasma associated with the burst of oscillation of magnetic field observed with magnetic probe arrays is characterized by the sudden decrease of neutron emission rate, central ion temperature, and kinetic energy of the plasma [51, 52].

A. Energetic particle driven MHD collapse

Toroidal Alfven Eigenmodes (TAEs) driven by the energetic particle are widely observed in tokamak and helical plasma when the fast ion pressure gradient is large enough [53–55]. Recently, the abrupt onset of the perturbation with the tongue-shaped topology (localized in poloidal and toroidal directions) which leads the sudden redistribution of energetic ion and MHD burst associated with the sudden increase of plasma rotation by the change in the radial electric field. This new type of MHD burst is characterized by a unique trigger mechanism. It is triggered by the tongue shaped deformation that appears between the low-order of a rational surfaces. MHD instability causing the tongue shaped deformation is highly non-linear and grows within one cycle and triggers the re-distribution and loss of energetic trapped ions, which are indicated by the sharp jump of RF intensity. The plasma starts to rotate after the loss of ions and MHD burst starts due to the resonance between the mode frequency and the precession frequency of the trapped particle.

As seen in figure 8(a)(b)(c), the repeated burst of magnetic field perturbation with large amplitude are observed with magnetic probes at toroidal angle of 90, 198, and 270 degrees [56], and are called MHD burst in LHD.

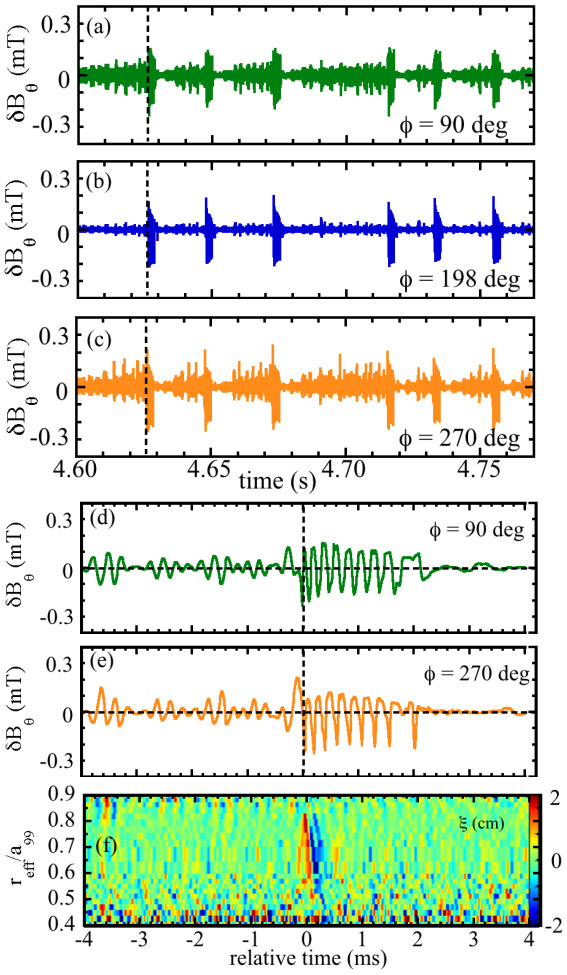

FIG. 8: (a) Time evolution of magnetic field perturbation measured with magnetic probes at toroidal angle of (a) 90, (b) 198, and (c) 270 degrees and expanded view of magnetic field perturbation (from 4ms before to 4ms after the collapse) at toroidal angle of (d) 90 and (e) 270 and contour of equi-temperature surface evaluated from ECE signal in LHD (from figure 1(a)(b)(c) in [7] and figure 1(a)(c) in [8] modified).

The similar magnitude of the oscillation amplitude in these three probes indicates that the MHD perturbations are rotating toroidally. However, the magnetic perturbation amplitude at 198 degree probes is much smaller than these at 90 and 270 degree probes between the MHD burst. This indicates that the MHD oscillation between the MHD burst is caused by the standing wave. Figure 8(d) (e) are expanded plots of magnetic perturbations from 4ms before to 4ms after the collapse, which is indicated by the sharp increase of the RF signal. The frequency of the MHD oscillation and MHD burst is $\sim$ 5 kHz, which is lower than the typical MHD frequency of Toroidal Alfven Eigenmodes (TAEs) in LHD ($\sim$ 70 kHz [55]). Different from the MHD burst driven by TAEs, the MHD burst starts associated with the plasma rotation driven by loss of energetic ions [7]. MHD burst is not the cause of energetic ions loss but the result of the plasma rotation driven by energetic ion loss. The oscillation of the magnetic field at 90 and 270 degree probes is out-of-phase and shows the $n = 1$ structure. Therefore, the mode between MHD burst is $n = 1$ stationary mode. In contrast, MHD burst (0 - 2ms after the collapse) shows phase delay in toroidal direction and indicates that this is n=1 rotating mode. It should be noted that the perturbation of the magnetic field 0.1ms before the collapse indicated by the vertical dashed line does not have $n = 1$ structure and the perturbation of the magnetic field is localized poloidally and toroidally.

Figure 8(f) shows the contour of displacement of equi-temperature surface evaluated from $\delta T_e/\nabla T_e$ measured with ECE signal. Here the positive value (red) stands for the outward displacement, while the negative value (blue) stands for the inward displacement. The positive displacement indicated with red starts between two rational surfaces of $\iota = 0.5$ at $r_{\rm eff}/a_{99} = 0.5$ and $\iota = 1$ at $r_{\rm eff}/a_{99} = 0.9$. The positive displacement propagates outward and then propagates inward. The negative displacement (blue) is also observed just after the outward displacement. The outward propagation of positive displacement is called tongue formation, and the inward propagation of positive and negative displacement is called tongue collapse [7].

These displacements at the tongue formation and collapse are much more significant than the displacement at the rational surfaces ($r_{\rm eff}/a_{99} = 0.5$ and 0.9.) and are not localized but are radially propagating. The displacement of the tongue-shaped deformation reaches up to 2cm at the end of the formation, which is much larger than the displacement (0.2 $\sim$ 0.5cm) observed at the two rational surfaces of $\iota = 0.5$ and 1.0 [57]. The tongue-shaped deformation typically quickly decays within one or a few cycles, while the displacement at the rational surface continues to oscillate. It should be noted that the perturbation of the magnetic field is correlated to the oscillation localized in the rational surface of $\iota = 1$ at $r_{\rm eff}/a_{99} = 0.9$ as seen in the few cycles in t = -3.5 ms. The perturbation of magnetic field due to tongue-shaped deformation has comparable magnitude to that of MHD oscillation localized at $r_{\rm eff}/a_{99} = 0.9$, although the displacement of tongue-shaped deformation is 4 times the displacement localized at $\iota = 1.0$ rational surface.

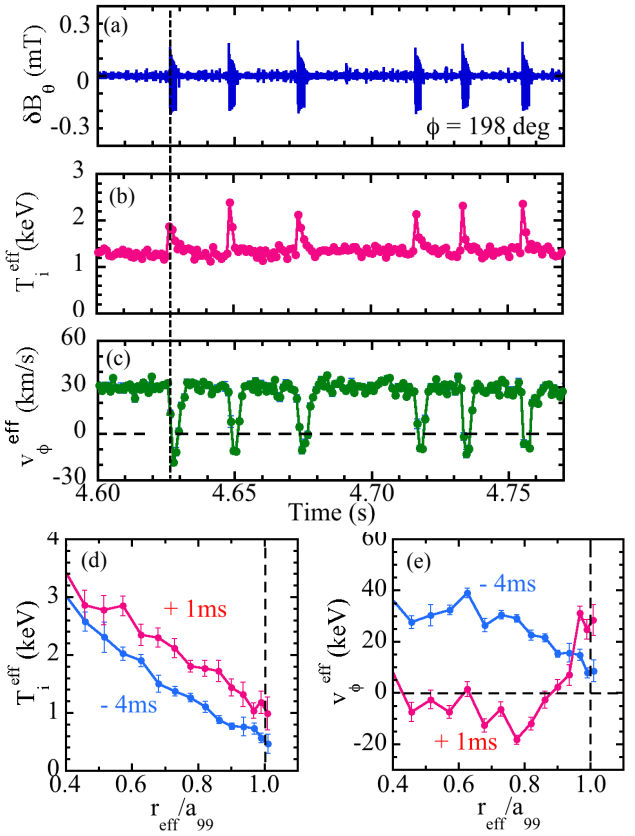

FIG. 9: (Time evolution of (a) perturbation of the magnetic field (effective ion temperature, (c) effective toroidal rotation velocity and the radial profile of (d) the effective ion temperature and (e) effective toroidal rotation velocity in LHD.

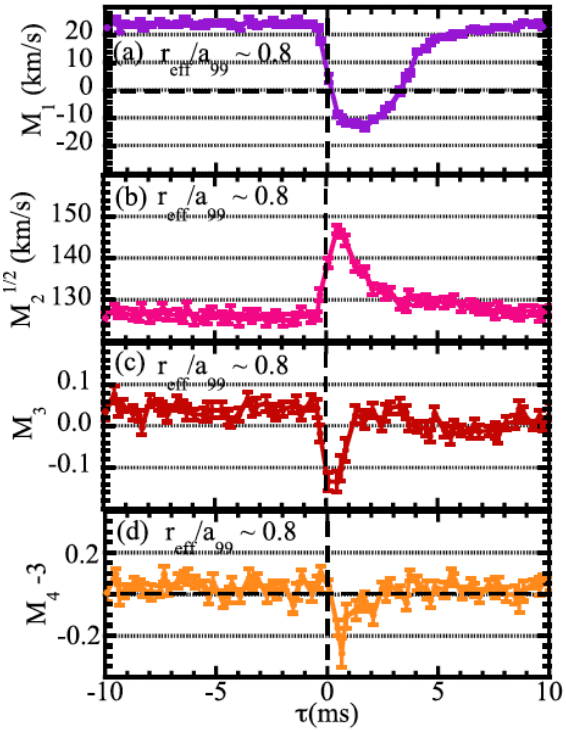

FIG. 10: Time evolution of (a) 1st moment (M_1), (b) square root of 2nd moment (M_2), (c) 3rd moment (M_3), and (d) 4th moment (M_4 - 3) of ion velocity distribution of carbon at $r_{\rm eff}/a_{99} = 0.8$, at the tongue event. Here τ is the relative time of the event with respect to the time of the sharp increase of RF intensity in LHD (from figure 4 in [9]).

B. Impact of tongue collapse on ion velocity distribution

The MHD burst triggered by the tongue collapse has a strong effect on plasma velocity distribution and alters the effective ion temperature and effective toroidal rotation velocity. At each MHD burst, the abrupt increase of effective ion temperature and increase of effective toroidal rotation velocity in the counter-direction is observed as seen in figure 9(a)(b)(c). The change of effective ion temperature and effective toroidal rotation velocity is within 1 ms and much faster than the transport time scale. This is due to the redistribution of ions in space, where the hot ions and counter-traveling ions in the core region ($r_{\rm eff}/a_{99} < 0.4$) move outward in a short time associated with the tongue formation and collapse. The increase of effective ion temperature and effective toroidal rotation velocity shows the relaxation in the ion-ion collision time scale.

Radial profiles of effective ion temperature and effective toroidal rotation velocity 4 ms before and 1 ms after the tongue collapse are plotted in figure 9(d)(e). The increase of effective ion temperature is 0.5 keV and relatively constant in space and ion temperature gradient is almost unchanged. Before the tongue collapse the effective toroidal rotation velocity is co-direction (parallel to equivalent plasma current direction) and it is in the counter-direction after the tongue collapse. The rapid change in the effective toroidal rotation velocity is the consequence of outward movement of counter-traveling particles, because the time scale of the change is much faster than the time scale of the momentum transport.

In order to investigate the mechanism for the rapid change of effective ion temperature and effective toroidal velocity, the distortion of ion velocity distribution from Maxwell-Boltzmann distribution is evaluated by the moment analysis of ion velocity distribution measured with charge exchange spectroscopy viewing the plasma toroidally [58]. The 0th to the 4th moment of ion velocity distributions are defined as

$$M_0 = \int f(v)dv \tag{4}$$

$$M_1 = \frac{1}{M_0}\int v f(v)dv \tag{5}$$

$$M_2 = \frac{1}{M_0}\int (v-M_1)^2 f(v)dv \tag{6}$$

$$M_3 = \frac{1}{M_0 M_2^{3/2}}\int (v-M_1)^3 f(v)dv \tag{7}$$

$$M_4 = \frac{1}{M_0 M_2^2}\int (v-M_1)^4 f(v)dv. \tag{8}$$

When the ion velocity distribution is Maxwell-Boltzmann distribution, $M_1 = V_\phi$, $M_2 = V_{\rm th}$, $M_3 = 0$, and M_4 - 3 = 0, where $V_{\rm th}$ is an ion thermal velocity. When the ion velocity distribution is distorted from Maxwell-Boltzmann distribution, M_3 and $M_4 - 1$ become non-zero.

The time evolutions of 1st moment (M_1), square root of 2nd moment (M_2), 3rd moment skewness (M_3), and 4th moment kurtosis (M_4 - 3) of ion velocity distribution of carbon at $r_{\rm eff}/a_{99} = 0.8$ are plotted in figure 10. Here τ is the relative time with respect to the tongue collapse indicated by the sharp increase of RF intensity. After the tongue collapse, 1st moment (M_1) and square root of the 2nd moment show the rapid change, which is consistent with the rapid increase of effective toroidal rotation velocity in counter-direction and the rapid increase of effective ion temperature. Before the tongue collapse, the 3rd moment is close to zero, which shows that the ion distribution is Maxwell-Boltzmann distribution. After the tongue collapse, M_3 value drops to -0.15 and recovers to zero within 1 - 2 ms. The change is much larger than the error bar of the measurements. The M_4 - 3 also shows the significant drop to -0.2 after the tongue collapse, The negative M_4 - 3 indicates the increase of epithermal ions due to the outward shift of hot ions towards the plasma edge. This negative M_4 - 3 also recovers to zero within 1 - 2 ms due to the thermalization of ion distribution through ion-ion collisions.

The outward shift of ions causes the intense negative radial electric field in the core region. The change in

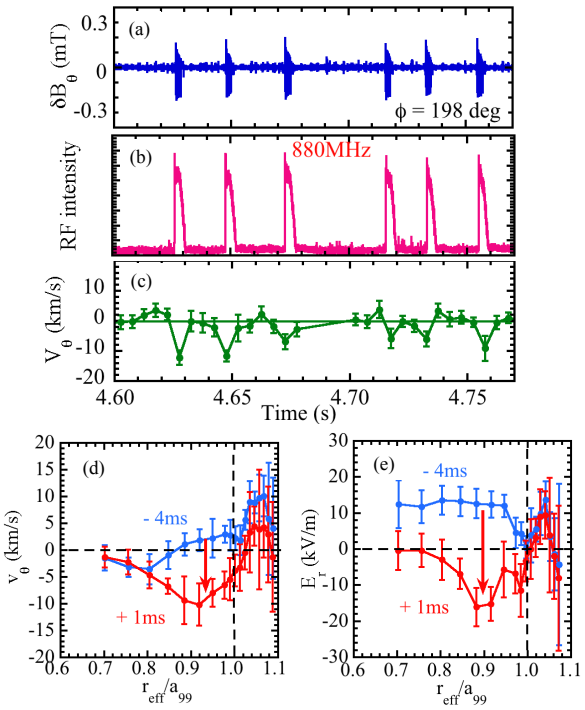

FIG. 11: Time evolution of (a) perturbation of the magnetic field, (b) RF intensity, and (c) poloidal rotation velocity, and radial profiles of (d) poloidal rotation velocity and (d) radial electric field in LHD.

the radial electric field is measured with charge exchange spectroscopy, while the timing of loss of ion is monitored by the RF probe. RF intensity measured with RF probe is a good time indicator of the ion loss, because the high frequency instability is excited when the iron in the hot core is exhausted to the plasma edge. Therefore, the intensity of RF radiation probes is used as a timing indicator for the energetic ion loss from the plasma[59] in this work because the RF probe has high time resolution and is sensitive to the high frequency RF signals excited by the loss of energetic ions at the plasma edge [60, 61]. Large poloidal flow in the electron diamagnetic direction and sharp increase of RF intensity is observed at each MHD burst as seen in figure 11(a) (b) (c).

The radial profile of poloidal rotation velocity and radial electric field shows the large negative electric field well at $r_{\rm eff}/a_{99} = 0.9$, while the radial electric field before the tongue collapse is positive as seen in figure 11(d)(e). The change in radial electric field near the plasma edge ($r_{\rm eff}/a_{99} > 0.8$) is mainly contributed by the change in poloidal flow in electron diamagnetic direction, while the change in radial electric field further inside the plasma

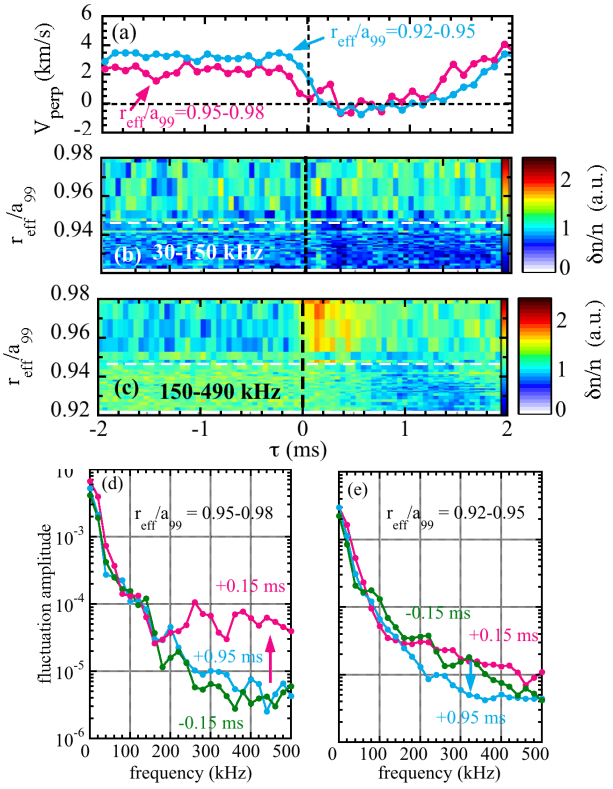

FIG. 12: (a) Time evolution of (a) perpendicular velocity at the edge stochastic region ($r_{\rm eff}/a_{99} > 0.95$) and inside plasma ($r_{\rm eff}/a_{99} < 0.95$) and contour of fluctuation level integrated (b) low frequency (30 - 150kHz) turbulence and (c) high frequency (150 - 490 kHz) turbulence and frequency spectrum at the edge stochastic region and inside plasma in LHD (from figure 3(b)(c)(g) and figure 4(c)(d) in [10]).

is contributed by increase of toroidal flow in counter-direction. The radial electric field outside plasma boundary ($r_{\rm eff}/a_{99} = 1$) is almost unchanged. The change of the radial profile of the radial electric field to more negative clearly shows the loss of bulk ions associated with the tongue collapse.

C. Turbulence exhaust driven by MHD collapse

It is interesting to investigate the impact of MHD collapse on turbulence. The Doppler reflectometer is a useful tool for measuring the density fluctuation near the plasma boundary. The frequency-hopping Doppler reflectometers have been installed in LHD and the frequency is set to 30 GHz in this experiment[62, 63]. The location of the measurement (reflection point) can be scanned from the edge stochastic region to the nested region inside during the discharge where the edge density gradually decreases in time. The analysis technique of the radial scan of the reflection point of the Doppler reflectometer using the density ramp up/down in time has been applied in LHD experiment. This method has been recognized to be a useful technique to measure the radial profile of density fluctuation amplitude and perpendicular velocity near the plasma edge[64].

Figure 12 shows time evolution of perpendicular velocity at the edge stochastic region ($r_{\rm eff}/a_{99} > 0.95$) and inside plasma ($r_{\rm eff}/a_{99} < 0.95$). The contour of fluctuation level integrated low frequency (30 - 150kHz) turbulence and high frequency (150 - 490 kHz) turbulence are also plotted. When the reflection point is in the edge stochastic region, the positive spikes of intensity of high frequency (f = 150 - 490 kHz) micro turbulence are observed at the tongue collapse event. In contrast, the slight decrease of high frequency micro turbulence is observed at the nested flux region inside the plasma ($r_{\rm eff}/a_{99} < 0.95$). It should be pointed out that there is no change in turbulence intensity at lower frequency range (f = 30 - 150 kHz).

The time evolution of perpendicular velocity of the stochastic region and the nested region inside shows the change of perpendicular velocity in the electron diamagnetic direction. This data indicates the formation of negative radial electric field consistent with the negative poloidal flow measured with charge exchange spectroscopy. The formation of a negative electric field is transient and lasts only 2 ms. As seen in the spectrum at stochastic region ($r_{\rm eff}/a_{99} > 0.95$) plotted in figure 12(d)(e), the micro turbulences only in the frequency region above 150 kHz increase rapidly within 0.15 ms after the collapse. This rapid increase of turbulence observed is due to the rapid avalanche like radial propagation process [65–68] into the SOL rather than the change in locally driven turbulence associated with the changes in temperature or density gradients in the SOL.

IV. DISCUSSION

As the example of interplay between the turbulence and the topology, the following experimental evidence has been reported in a toroidal plasma. Turbulence spreading from the X-point to the O-point of the magnetic island is identified from the phase delay between heat pulse and turbulence response. The bifurcation of magnetic island states can be explained by the interplay between turbulence spreading and stochastization at X-point of the magnetic island. The radial propagation of the stochastic magnetic field towards the magnetic axis of helical plasma can be also explained by the interplay between the plasma flow and stochastization of the magnetic field.

The experimental evidence for two states of a magnetic

island provides a new insight into understanding the radial flux of (surface-averaged) heat transport in the presence of magnetic islands during RMP experiments. This understanding can be further improved and it may be possible to achieve better control of the heat transport in discharges with RMP fields by using the heat pulse propagation technique as a tool to identify the state of the magnetic island. Turbulence spreading observed in the magnetic island also gives a new insight on turbulence spreading physics which is necessary for the better understanding of turbulence in the SOL, where the spreading turbulence dominates locally driven turbulence. Because the turbulence in the SOL is beneficial for the broadening of the power decay length, deeper understanding of SOL turbulence is essential for better control of the SOL decay length in future device. The impact of magnetic field stochastization on turbulence spreading and flow damping explore new research fields. The former is important in understanding the complicated plasma response of particle and heat transport to the RMP field and the latter is indispensable to understand the response of plasma flow to RMP fields, where partial stochastization is expected. Better understanding of the impact of RMP fields on plasma flow is essential for the more reliable prediction of power threshold of the L to H-mode transition in future device.

The strong impact of energetic particles driven MHD instability has been observed. MHD bursts are triggered by the tongue formation and collapse. This tongue collapse has an impact of ion velocity distribution and causes the distortion from Maxwell-Boltzmann distribution. The distortion has been found in experiments with a significant transient change in skewness and kurtosis of ion velocity distribution. The tongue collapse also enhances the loss of bulk ions of epithermal ions and produces the negative radial electric field and excite the MHD instability at the plasma edge. The turbulence exhaust by the tongue collapse is also observed in the Doppler reflectometer. This interplay between MHD and turbulence is essential for the integrated understanding for various phenomena in toroidal plasma.

Understanding the impact of MHD instabilities driven by energetic particles on plasma flow and turbulence becomes more important for future devices, because a increased fraction of energetic particles is expected in burning plasmas. Because of the strong coupling between plasma rotation and the plasma potential in toroidal plasma, the plasma rotation can be driven by energetic ion losses triggered by MHD instabilities. Once the plasma starts to rotate, another MHD instability can be excited by the resonance between the mode frequency and the precession frequency of the trapped particles. This is an example where an MHD instability drives another MHD instability through the plasma flow which is determined by the momentum transport. Therefore, the interplay between MHD and transport is a key physics in understanding the situation where various MHD modes appear one after the other during the discharge in the plasma where the fraction of beam beta is high [16, 69].

V. ACKNOWLEDGMENTS

The author wishes to thank LHD Experiment Group and DIII-D team for their excellent support of this work and Dr. T.E. Evans (GA) for his useful comments. This work is supported by the National Institute for Fusion Science grant administrative budgets (NIFS10ULHH021,NIFS17KLPH030) and JSPS KAKENHI Grant Numbers JP15H02336, JP16H02442, JP17H01368.

[1] Shibata K., and Tanuma, S.,*Earth Planets Space* **53**, 473 (2001).
[2] Nishizuka N., and Shibata, K., *Phys. Rev. Lett.* **110**, 051101 (2013).
[3] Biancalani A., *et al.* Interaction of Alfvénic modes and turbulence, investigated in a self-consistent gyrokinetic framework, 46th EPS Conference on Plasma Physics (Milano, Italy, 8-12 July, 2019)
[4] Ida, K., *et al. Phys. Rev. Lett.* **120** 245001 (2018).
[5] Ida, K., *et al. Sci. Rep.* **5** 16165 (2015).
[6] Ida, K., *et al. Nat. Commun.* **6** 5816 (2015).
[7] Ida, K., *et al. Sci. Rep.* **8** 2804 (2018).
[8] Ida, K., *et al. Sci. Rep.* **6** 36217 (2016).
[9] Ida, K., *et al. Phys. Plasmas* **24** 122502 (2017).
[10] Ida, K., *et al. Nucl. Fusion* **58** 112008 (2018).
[11] Yun, G. S., *et al. Phys. Rev. Lett.* **107**, 045004 (2011).
[12] Lee, J. E., *et al. Sci. Rep.* **7**, 45075 (2017).
[13] Evans T.E. *et al.* 2018 arXiv:1805.10394v2.
[14] Wu, W. *et al. Nucl. Fusion* **59** 066010 (2019).
[15] Ida, K., *et al. Nucl. Fusion* **55** 013022 (2015).
[16] Ida K., *Nucl. Fusion* **59** (2019) in press.
[17] Happel, T., *et al. J. Nucl. Mat.* **18** 159 (2019).
[18] Harrison, J.R., *et al. Nucl. Fusion* **59** 112011 (2019).
[19] Harrison J. R. ,*et al. Phys. Plasmas* **22** 092508 (2015).
[20] Scotti F., *et al. Nucl. Fusion* **58** 126028 (2018).
[21] Kaye, S.M., *et al. Nucl. Fusion* **59** 112007 (2019).
[22] Grenfell, G., *et al. Nucl Fusion* **59** 016018 (2019).
[23] Snape, J. *et. al.*, *Plasma Phys. Control. Fusion.* **54** 085001 (2012).
[24] Inagaki S., *et. al.*, *Phys. Rev. Lett.* **92**, 055002 (2004).
[25] Bardóczi L. , *et. al.*, *Phys. Plasmas* **24**, 062503 (2017).
[26] T Hahm . S., *et. al.*, *Plasma Phys. Control. Fusion.* **46**, A323 (2004).
[27] Diamond P.,H. and Hahm T. S. , *J. Korean Phys. Soc,* **73** 747 (2018).
[28] Fonck R J, *et al.* 1990 *Rev. Sci. Instrum.* **61** 3487 (1990).
[29] McKee G R, *et al. Plasma Fusion Res.* **2** s1025 (2007).
[30] Evans T. E. , Moyer R. A. and Monat P., *Phys. Plasmas* **9** 4957 (2002).
[31] Ida, K., *et al. Nucl Fusion* **56** 092001 (2016).

[32] Wang W.X., Hahm T.S., Lee W.W., Rewoldt G., Manickam J. and Tang W.M. *Phys. Plasmas* **14** 072306 (2007).
[33] Yi S., Kwon J.M., Diamond P.H. and Hahm T.S. *Nucl. Fusion* **55** 092002 (2015).
[34] Diamond, P.H., Dupree, T.H., Tetreault, D.J., *Phys. Rev. Lett.* **45**, 562 (1980).
[35] Lichtenberg, A.J., Itoh, K., Itoh, S.-I., Fukuyama, A., *Nucl. Fusion* **32**, 495 (1992).
[36] Itoh, K., Itoh, S.-I., Fukuyama, A., Lichtenberg, A.J., *Nucl. Fusion* **32**, 1851 (1992).
[37] Liang, Y., *et al. Nucl. Fusion* **47**, L21 (2007).
[38] Ida K., *et al. Phys. Rev. Lett.* **100** 045003 (2008).
[39] Ida, K., *et al. New J. Phys.* **15**, 013061 (2013).
[40] Ida, K., *et al. Plasma Phys. Control. Fusion.* **57** 014036 (2015).
[41] Terry, P. W. *et al. Phys. Plasmas* **3** 1999 (1996).
[42] Ida, K., *et al. Nucl. Fusion* **57** 076032 (2017).
[43] Cheng C.Z. and Chance M.S., *Phys. Fluids* **29**, 3695 (1986).
[44] Chen L. , *Phys. Plasmas* **1**, 1519 (1994).
[45] Wong K.L., *Plasma Phys. Control. Fusion.* **41**, R1 (1999).
[46] Heidbrink W.W. , *Phys. Plasmas* **15**, 055501 (2008).
[47] Toi, K., *et al. Nucl. Fusion* **40**, 1349 - 1362 (2000).
[48] Yamamoto, S., *et al. Nucl. Fusion* **45**, 326 - 336 (2005).
[49] Nagaoka, K., *et al. Phys. Rev. Lett.* **100**, 065005 (2008).
[50] Ogawa, K., *et al. Nucl. Fusion* **50**, 084005 (2010).
[51] Ogawa, K., *et al. Nucl. Fusion* **58** 044001 (2018).
[52] Ogawa, K., *et al.Plasma Phys. Control. Fusion.* **60** 044005 (2018).
[53] Gryaznevich, M.P., *et al. Nucl. Fusion* **48** 084003 (2008).
[54] Fredrickson, E.D., *et al. Nucl. Fusion* **53** 013006 (2013).
[55] Ogawa, K., *et al. Nucl. Fusion* **53** 053012 (2013).
[56] Sakakibara, S., *et al. Fusion Sci. Technol.* **58**, 471-481 (2010).
[57] Voermans, S., *et al. Nucl. Fusion* **59** 106041 (2019).
[58] Yoshinuma M., *et al. Fusion Sci. Technol.* **58**, 375 (2010).
[59] Heidbrink, W.W., *et al. Plasma Phys. Control. Fusion.* **53**, 085028 (2011).
[60] Schild, P., Cottrell, G.A., and Dendy, R.O., *Nucl. Fusion* **29**, 834 (1989).
[61] Dendy, R.O., Lashmore-Davies, C.N., McClements, K. G., *et al. Phys. Plasmas* **1**, 1918 (1994).
[62] Tokuzawa, T., Ejiri, A., and Kawahata, K., *Rev. Sci. Instrum.* **81**, 10D906 (2010).
[63] Tokuzawa, T., *et al. Rev. Sci. Instrum.* **83**, 10E322 (2012).
[64] Creely, A.J., Ida, K., Yoshinuma, M., *et al. Rev. Sci. Instrum.* **88**, 073509 (2017).
[65] Diamond, P. H. and Hahm T. S. 1995 *Phys. Plasmas* **2** 3640.
[66] Carreras B. A., Newman D., Lynch V. E., and Diamond P. H. *Phys. Plasmas* **3** 2903 (1996).
[67] Newman D. E., Carreras B.A., Diamond P. H. and Hahm T. S. *Phys. Plasmas* **3** 1858 (1996).
[68] Garbet X. and Waltz R. E. *Phys. Plasmas* **5** 2836 (1998).
[69] Lauber PH. *et al.* Strongly non-linear energetic particle dynamics in ASDEX Upgrade scenarios with core impurity accumulation. Preprint: 2018 IAEA Fusion Energy Conf. (Gandhinagar, India, 22-27 October 2018) [EX/1-1]. https://www.iaea.org/events/fec-2018.